The structure and chemistry of the TiO_2-rich surface of $SrTiO_3$ (001)

Natasha Erdman*, Kenneth R. Poeppelmeier†, Mark Asta‡, Oliver Warschkow§, Donald E. Ellis§ & Laurence D. Marks*

** Department of Materials Science and Engineering, Institute for Environmental Catalysis; † Department of Chemistry, Institute for Environmental Catalysis; ‡ Department of Materials Science and Engineering; and § Department of Physics and Astronomy, Institute for Environmental Catalysis, Northwestern University, Evanston, Illinois 60208-3108, USA*

Oxide surfaces are important for applications in catalysis and thin film growth. An important frontier in solid-state inorganic chemistry is the prediction of the surface structure of an oxide. Comparatively little is known about atomic arrangements at oxide surfaces at present, and there has been considerable discussion concerning the forces that control such arrangements. For instance, one model suggests that the dominant factor is a reduction of Coulomb forces[1]; another favours minimization of 'dangling bonds' by charge transfer to states below the Fermi energy[2]. The surface structure and properties of $SrTiO_3$—a standard model for oxides with a perovskite structure—have been studied extensively[3–14]. Here we report a solution of the 2×1 $SrTiO_3$ (001) surface structure obtained through a combination of high-resolution electron microscopy and theoretical direct methods. Our results indicate that surface rearrangement of TiO_{6-x} units into edge-sharing blocks determines the SrO-deficient surface structure of $SrTiO_3$. We suggest that this structural concept can be extended to perovskite surfaces in general.

$SrTiO_3$ has been used as a substrate for epitaxial growth of superconducting thin films[13] and a buffer layer for the growth of GaAs thin films on Si[14]. The structure of $SrTiO_3$ can be described as a close-packed lattice of oxygen and strontium in a 3:1 ratio, with titanium in octahedral interstitial sites. For an ideal bulk-terminated (001) surface, two configurations are possible: (1) Ti and O termination with a ratio of 1:2 (TiO_2 stoichiometry); or (2) Sr and O termination with a ratio of 1:1 (essentially SrO). However, under various conditions (of atmosphere, pressure and temperature) transition metal oxides can exhibit different valences and coordination numbers, so the structure is actually more complex. Depending upon the experimental environment, under oxidative conditions 2×1, 4×2 and 6×2 surface reconstructions of $SrTiO_3$ have been reported[4–8] together with more complicated structures obtained by annealing in vacuum under reducing conditions[9,10]. In many cases the results are inconclusive and contradictory, and only a few studies have attempted to generate a model for these surface structures.

Diffraction techniques provide a powerful tool for the solution of surface structures and refinement of atomic positions. In a diffraction experiment, the amplitudes of the reflections are recorded, but the phase information is lost, preventing a direct Fourier inversion of the data. Our approach[15–18] solves the phase problem by exploiting probability relationships between the amplitudes and the phases of the diffracted beams. The algorithm searches for the set of phases with the lowest figures of merit (FOM), which are then used to create scattering potential maps that obey the imposed symmetry. Effectively, a set of plausible solutions for the structure is generated, starting only from the intensity data. If the experimental errors are very small, these maps can approach an accurate restoration. For surface data, provided that the sample is tilted off the zone axis, the intensities are more than 90% kinematical[19] and high-quality maps can generally be obtained. The method has already been used with either surface electron or X-ray diffraction data to solve more than 20 different surface structures using experimental data, more than half of which had not previously been solved. There are some subtle issues in using this approach to solve for surface structures, which are described in more detail elsewhere[15,16].

Starting with a single-crystal $SrTiO_3$ (001) wafer (99.95% pure), 3-mm disks were cut using an ultrasonic cutter. These were mechanically polished to a thickness of about 120 μm, dimpled, then ion milled with 4.8-kV Ar^+ ions using a Gatan precision ion polishing system (PIPS) to produce an electron-transparent sample. The sample was annealed in a tube furnace at 950–1,000 °C with a constant flow of high-purity oxygen to eliminate the damage caused by ion milling and to obtain the 2×1 reconstruction. Annealing at lower or higher temperatures produces the 4×2 and 6×2 reconstructions respectively, which we do not discuss here. These results were highly reproducible, indicating that the 2×1 structure observed is thermodynamically stable. Off-zone-axis electron diffraction patterns and bright-field images were obtained using the ultrahigh vacuum (UHV)-H9000 Hitachi electron microscope[20], operated at 300 kV at Northwestern University. For high-resolution electron microscopy (HREM) the samples were tilted to the zone axis and images were recorded using a JEOL-4010 electron microscope operated at 400 kV at Argonne National Laboratory.

Figure 1 shows an off-zone-axis selected area diffraction pattern with both 2×1 and 1×2 domains (marked on the figure) combined with a bright-field image of the $SrTiO_3$ (001) sample. The bright-field image indicates the formation of large flat ⟨100⟩ facets at the surface of the sample after annealing. Both high-resolution images and the theoretical direct methods yielded the same general solution to the surface structure; for clarity we describe the images first. Figure 2a shows a high-resolution image of a mainly single-domain 2×1 surface and a corresponding power spectrum. The image was noise-filtered using a Wiener filter[21] and the bulk contribution suppressed, similar to the strategies used previously[22,23]. Figure 2b displays the same image after lattice averaging (left) and after filtering to separate translation/inversion domains of the structure (right) on the top and bottom surfaces (for more details see ref. 23) with an image simulation inset in the centre. The images show a dominant structural motif, a zig-zag row of features with a local *p2mg* symmetry. Numerical image simulations (inset in Fig. 2b) were in fairly good agreement with the experimental data, with black dots corresponding to surface titanium sites. Among the plausible solutions determined by direct methods, only those

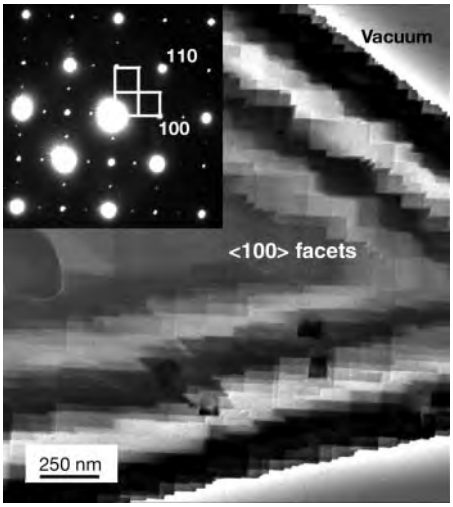

Figure 1 Bright-field image and off-zone-axis diffraction pattern (inset) of the (2×1) $SrTiO_3$ (001) surface, taken using the UHV-H9000 Hitachi transmission electron microscope (TEM). The surface unit cell for both domains of the reconstruction is marked.

containing the same structural element (for example, Fig. 3) were stable to subsequent refinements. Analysis indicated that these were Ti atom sites (not O or Sr), and using conventional difference maps combined with χ^2 refinements we were able to determine the oxygen sites.

The refinement of the structure against the diffraction data gave both the Ti and O atom positions, with a $\chi^2 = 2.01$. Alternative models of the structure, for example O addition on top of the Ti atoms, were considered, but the refinement results were significantly inferior.

The two-dimensional nature of the diffraction data does not allow refinement of the *z* position, so plane-wave pseudo-potential density functional (DFT) calculations[24–27] on a 13-layer slab model were employed as an independent structure refinement in three dimensions, starting from the experimentally obtained atomic positions. The calculation confirmed the *x*,*y* positions obtained from the χ^2 refinement, as well as relaxing the structure in the *z* direction (see Supplementary Information for atom positions and partial charges). Figure 4 shows the solution of the 2×1 $SrTiO_3$ surface structure. The top layer has a TiO_2 stoichiometry, with half of the TiO_5 units displaced along the [110] direction. The result is a row of 5-coordinated TiO_5 units that share edges between them as well as with the layer underneath, which is a part of the first full intact TiO_2 layer of $SrTiO_3$ with 6-coordinated Ti atoms. We note the tilting of the TiO_6 octahedra in the bulk layers underneath to support the reconstruction. In the surface layer we can distinguish between two different types of O atoms: (1) 'internal' O atoms (O1, O2) tightly bound inside the surface rows and shared between the octahedra; and (2) 'external' O atoms (O3, O4), not shared between the octahedra. The distances between the surface Ti atoms to the two external O atoms are significantly shorter than the bulk Ti–O distances (1.51 Å and 1.76 Å versus 1.95 Å), whereas the distance between the internal oxygens to surface Ti is bulk-like. Apparently the surface Ti atoms compensate for the lower coordination number by stronger bonding to the external oxygens. We further employed near-minimal basis linear combination of atomic orbitals (LCAO) DFT calculations[28] to obtain partial atomic charges. In support of the above argument, the charge analysis finds that the surface Ti and internal O atoms are bulk-like (Ti +2.0, O −1.2), whereas the charges on the two external O atoms are significantly reduced (O3 −0.8 and O4 −0.6 compared with −1.2 in the bulk), which is indicative of increased covalence.

$SrTiO_3$ is representative of a large class of oxides with the perovskite structure; it is therefore important to understand the basic character of its surfaces because similar considerations will apply to other materials. It is well established that the coordination chemistry of perovskite structures is dominated by the formation of corner-shared octahedral building blocks, along with large cations to achieve the appropriate stoichiometry. In an ABO_3 structure the A cation prevents any structural rearrangement at the surface. Without these large cations, the ReO_3-type structure is created, which can have corner as well as edge-shared octahedra; this means additional degrees of freedom for structural rearrangements. On chemical grounds, we therefore expect that the surface of a perovskite will rearrange to a BO_{3-x} configuration, effectively screening the B cations, while also minimizing surface dipoles and maximizing the coordination.

The surface structure reflects these concepts and is a hybrid of three components: (1) The first component is a linear structure involving two Ti atoms (Ti1 and Ti2) and two O atoms (O1 and O2), with essentially bulk-like electronic structure similar to edge-shared octahedral units, where each O atom is coordinated to 3 or 4 Ti atoms. (2) The second component consists of two external O atoms (O3 and O4) with much more covalent character, particularly O4 which is double-bonded to Ti1; the coordination number for each of the external O atoms is 1 or 2. (3) The third component is

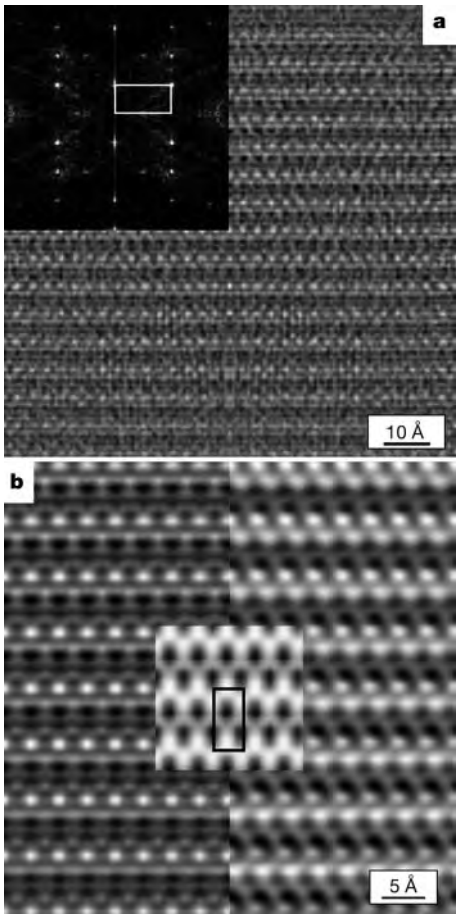

Figure 2 High-resolution image of the 2×1 $SrTiO_3$ (001) surface. Image was obtained with the JEOL-4010 TEM at Argonne National Laboratory. **a**, The image after being Wiener-filtered[23] and the bulk spots digitally removed. The inset shows the corresponding power spectrum, with unit cell marked. **b**, Enlarged translation-averaged image of the 2×1 structure (left) and after filtering to separate translation/inversion domains on the top and bottom surface (right). The inset shows a multislice simulation of the structure (defocus −55 nm) with the unit cell marked. The strong black features correlate with the positions of Ti atoms at the surface.

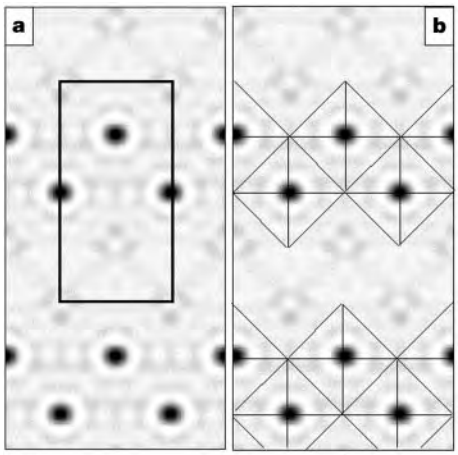

Figure 3 Theoretical direct methods solution of the (2×1) structure. **a**, Scattering potential map calculated from two-dimensional code for *pm* symmetry. **b**, Interpretation of the map in terms of TiO_x units. The primitive unit cell is indicated with solid lines ($a = 3.905$ Å, $b = 7.81$ Å, $\alpha = 90°$). In both cases regions of high potential—that is, possible atomic sites—are black, and subsequent analysis demonstrated that these were Ti atoms.

a slightly distorted bulk-like TiO_2-layer-terminated $SrTiO_3$ subsurface.

We note the retention of edge-shared TiO_5 units, yielding a charge-neutral reconstructed surface with the stoichiometry Ti_2O_4. Preliminary results for the 4×2 and the 6×2 $SrTiO_3$ surface structures show similar structural motifs, and suggest similar surface rearrangements. These results indicate that edge-shared assembly of TiO_x units on the surface, analogous to creation of 'block structures' in Nb_2O_{5-x} and other ReO_3-type bulk oxide structures, provides additional modes for rearrangement to lower-energy configurations and controls the surface structure of $SrTiO_3$.

We suggest that this structure formation rule can be extended to perovskites in general. We could compare this result for perovskite surfaces with the rules of sp^3 bonding for semiconductor surfaces, an idea first suggested for Si surfaces that quickly became widely used to explain surface structure formation in other semiconductors. This suggests that many of the concepts of bulk chemistry can also be applied to surfaces, coupled with minimizing surface dipole moments and maximizing coordination. Different specific results will occur, depending upon the bonding character and structural rules, for instance, delocalized electron states in metals, directional sp^2 or sp^3 in many semiconductors and block structures in oxides. □

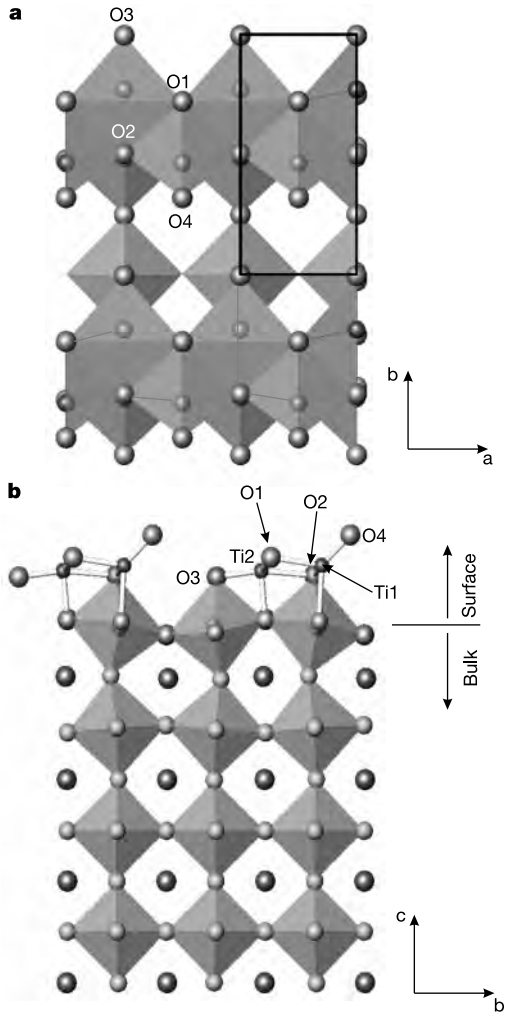

Figure 4 The 2×1 $SrTiO_3$ (001) surface structure. **a**, Top view; **b**, side view. TiO_x units are shown as partially filled octahedra on the surface; the primitive unit cell is indicated with solid lines ($a = 3.905$ Å, $b = 7.81$ Å).

Methods

Diffraction analysis

A series of negatives with exposure times varying from 0.5 s to 120 s were recorded for the 2×1 reconstruction using strategies that we have developed over the past decade[29]. The negatives were digitized to eight bits with a 25-μm pixel size using an Optronics P-1000 microdensitometer, and intensities extracted using a cross-correlation technique[30], then averaged using a *p2mm* Patterson plane group symmetry to yield 18 independent intensities. (Under the exposure conditions used, the intensity readout from the microdensitometer was proportional to the true intensities of the diffraction spots.) Because *p2mm* Patterson symmetry may correspond to *pm*, *pg*, *p2mm*, *p2mg* or *p2gg* plane group symmetries, all were tested in the calculations. Final structure refinement was performed based on χ^2, defined as:

$$\chi^2 = (N - M)^{-1} \sum [(I_{meas} - I_{calc})/\sigma]^2 \quad (1)$$

where I_{calc} is the calculated intensity, I_{meas} the measured intensity, N the number of data points, M the number of variable parameters, and σ the measurement error.

Electronic structure

DFT calculations were performed using the *ab initio* total-energy and molecular-dynamics program VASP (Vienna *ab initio* simulation package) developed at the Institut fur Material-physik of the Universität Wien[24–27], employing the generalized-gradient approximation[27]. The VASP code uses ultrasoft pseudopotentials[26] and a plane-wave expansion of the electronic wave functions.

Received 22 May; accepted 23 July 2002; doi:10.1038/nature01010.

1. Wolf, D. Reconstruction of NaCl surfaces from a dipolar solution to the Madelung problem. *Phys. Rev. Lett.* **68,** 3315–3318 (1992).
2. Pashley, M. D. Electron counting model and its application to island structures on molecular-beam epitaxy grown GaAs(001) and ZnSe(001). *Phys. Rev. B* **40,** 10481–10487 (1998).
3. Kawasaki, M. *et al.* Atomic control of the $SrTiO_3$ crystal-surface. *Science* **266,** 1540–1542 (1994).
4. Cord, B. & Courths, R. Electronic study of $SrTiO_3$ surfaces by photoemission. *Surf. Sci.* **162,** 34–38 (1985).
5. Jiang, Q. D. & Zegenhagen, J. c(6 × 2) and c(4 × 2) reconstruction of $SrTiO_3$ (001). *Surf. Sci.* **425,** 343–354 (1999).
6. Naito, M. & Sato, H. Reflection high-energy electron diffraction study on the $SrTiO_3$ surface structure. *Physica C* **229,** 1–11 (1994).
7. Jiang, Q. D. & Zegenhagen, J. SrTiO3 (001)-c(6 × 2): A long-range, atomically ordered surface stable in oxygen and ambient air. *Surf. Sci.* **367,** L42–L46 (1996).
8. Nishimura, T., Ikeda, A., Namba, H., Morishita, T. & Kido, S. Structure change of TiO_2-terminated $SrTiO_3$ (001) surfaces by annealing in O_2 atmosphere and ultra-high vacuum. *Surf. Sci.* **421,** 273–278 (1999).
9. Liang, Y. & Bonnell, D. A. Atomic structures of reduced $SrTiO_3$ (001) surfaces. *Surf. Sci. Lett.* **285,** L510–L516 (1993).
10. Matsumoto, T., Tanaka, H., Kawai, T. & Kawai, S. STM-imaging of a $SrTiO_3$ (100) surface with atomic-scale resolution. *Surf. Sci.* **278,** L153–L158 (1992).
11. Szot, K. & Speier, W. Surfaces of reduced and oxidized $SrTiO_3$ from atomic force microscopy. *Phys. Rev. B* **60,** 5909–5926 (1999).
12. Padilla, J. & Vanderbilt, D. *Ab initio* study of $SrTiO_3$. *Surf. Sci.* **418,** 64–70 (1998).
13. Aruta, C. Structure of superconducting $[BaCuO_x]_2/[CaCuO2]_n$ superlattices on $SrTiO_3$ (001) investigated by X-ray scattering. *Phys. Status Solidi A* **183,** 353–364 (2001).
14. Droopard, R. *et al.* Development of high dielectric constant epitaxial oxides on silicon by molecular beam epitaxy. *Mater. Sci. Eng. B* **87,** 292–296 (2001).
15. Marks, L. D. *et al.* Direct methods for surfaces. *Surf. Rev. Lett.* **5,** 1087–1106 (1998).
16. Marks, L. D., Erdman, N. & Subramanian, A. Crystallographic direct methods for surfaces. *J. Phys. Condens. Matter* **13,** 10677–10688 (2001).
17. Collazo-Davila, C., Grozea, D. & Marks, L. D. Determination and refinement of the Ag/Si(111)-(3 × 1) surface structure. *Phys. Rev. Lett.* **80,** 1678–1681 (1998).
18. Marks, L. D., Sinkler, W. & Landree, E. A feasible set approach to the crystallographic phase problem. *Acta Cryst.* **55,** 601–612 (1999).
19. Xu, P. & Marks, L. D. Intensities of surface diffraction spots in plan view. *Ultramicroscopy* **45,** 155–157 (1992).
20. Collazo-Davila, C. *et al.* Design and initial performance of an ultrahigh vacuum Sample Preparation Evaluation Analysis and Reaction (SPEAR) system. *J. Microsc. Soc. Am.* **1,** 267–279 (1995).
21. Marks, L. D. Wiener-filter enhancement of noisy HREM images. *Ultramicroscopy* **62,** 43–52 (1996).
22. Marks, L. D. & Plass, R. Atomic-structure of Si(111)-(5 × 2)-Au from high resolution electron microscopy and heavy-atom holography. *Phys. Rev. Lett.* **75,** 2172–2175 (1995).
23. Bengu, E. *et al.* Imaging the dimers in Si(111)-(7 × 7). *Phys. Rev. Lett.* **77,** 4226–4228 (1996).
24. Kresse, G. & Hafner, J. *Ab-initio* molecular dynamics for liquid metals. *Phys. Rev. B* **47,** 558–561 (1993).
25. Kresse, G. & Furthmuller, J. Efficient iterative schemes for *ab initio* total-energy calculations using a plane-wave basis set. *Phys. Rev. B* **54,** 11169–11186 (1996).
26. Vanderbilt, D. Soft self-consistent pseudopotentials in a generalized eigenvalue problem. *Phys. Rev. B* **41,** 7892–7895 (1990).
27. Perdew, J. P. in *Electronic Structure of Solids '91* (eds Ziesche, P. & Eschrig, H.) 11 (Akademie, Berlin, 1991).
28. Warschkow, O., Dyke, J. M. & Ellis, D. E. A divide-and-conquer implementation of the discrete variational DFT method for large molecular and solid systems. *J. Comp. Phys.* **143,** 70–89 (1998).
29. Jayaram, G., Xu, P. & Marks, L. D. Atomic structure of the Si (001) 2 × 1 surface. *Phys. Rev. Lett.* **71,** 3489–3492 (1993).
30. Xu, P., Jayaram, G. & Marks, L. D. Cross-correlation method for intensity measurement of transmission electron-diffraction patterns. *Ultramicroscopy* **53,** 15–18 (1994).

Supplementary Information accompanies the paper on *Nature*'s website (http://www.nature.com/nature).

Acknowledgements

HREM analysis was carried out at the Electron Microscopy Collaborative Research Center at Argonne National Laboratory. This work was supported by the EMSI program of the National Science Foundation and the US Department of Energy Office of Science at the Northwestern University Institute for Environmental Catalysis. M.A. acknowledges funding from the National Science Foundation.

Competing interests statement

The authors declare that they have no competing financial interests.

Correspondence and requests for materials should be addressed to L.D.M. (e-mail: l-marks@northwestern.edu).

Evidence from the AD 2000 Izu islands earthquake swarm that stressing rate governs seismicity

Shinji Toda*, Ross S. Stein† & Takeshi Sagiya‡

** Active Fault Research Center, Geological Survey of Japan, AIST, Tsukuba 305-8567, Japan*
† US Geological Survey, MS 977, Menlo Park, California 94025, USA
‡ Geographical Survey Institute, Tsukuba 305-0811, Japan

Magma intrusions and eruptions commonly produce abrupt changes in seismicity far from magma conduits[1–4] that cannot be associated with the diffusion of pore fluids or heat[5]. Such 'swarm' seismicity also migrates with time, and often exhibits a 'dog-bone'-shaped distribution[3,4,6–9]. The largest earthquakes in swarms produce aftershocks that obey an Omori-type (exponential) temporal decay[10–12], but the duration of the aftershock sequences is drastically reduced, relative to normal earthquake activity[7,13]. Here we use one of the most energetic swarms ever recorded to study the dependence of these properties on the stress imparted by a magma intrusion[8,11,14,15]. A 1,000-fold increase in seismicity rate and a 1,000-fold decrease in aftershock duration occurred during the two-month-long dyke intrusion. We find that the seismicity rate is proportional to the calculated stressing rate, and that the duration of aftershock sequences is inversely proportional to the stressing rate. This behaviour is in accord with a laboratory-based rate/state constitutive law[16], suggesting an explanation for the occurrence of earthquake swarms. Any sustained increase in stressing rate—whether due to an intrusion, extrusion or creep event—should produce such seismological behaviour.

The swarm struck the Izu volcanic islands 150 km south of Tokyo, producing 7,000 shocks with magnitude $M \geq 3$, and five $M \geq 6$ shocks; the total seismic energy release was 1.5×10^4 J, nearly an order of magnitude larger than the swarms that occurred in 1965–67 at Matsushiro, Japan, or in 1980 in Long Valley, California. The Izu swarm was accompanied by five phreatic eruptions of Miyakejima. Seismic activity began on 26 June with a shallow, dense swarm under Miyakejima, and migrated northwest (Fig. 1a). In July, the swarm developed northern and southern lobes (Fig. 1c, d). Earthquakes with $M = 6.4$ (1 July), $M = 6.1$ (9 July) and $M = 6.0$ (18 August) struck near the centre of the swarm, and $M = 6.3$ (15 July) and $M = 6.4$ (30 July) shocks struck ~25 km from the centre. Although it is generally assumed that the duration of aftershock sequences is proportional to mainshock magnitude[10], aftershocks of these $M \approx 6$ strike-slip earthquakes persisted for as little as a day, whereas aftershocks of $M = 6$ events normally last several years in the Izu islands (Fig. 2a). The distance between Kozushima and Shikinejima gradually extended by 0.85 m until 23 August, when the seismicity and rapid displacement ceased[17] (Fig. 3a).

The seismicity and deformation data are most compatible with a laterally propagating dyke intrusion, a process common to the Izu peninsula[8,9,18]. We assume that a vertical dyke propagated to its full length in the first week (Fig. 1a), and then opened continuously for seven weeks. We infer 20 m of expansion over a depth extent of

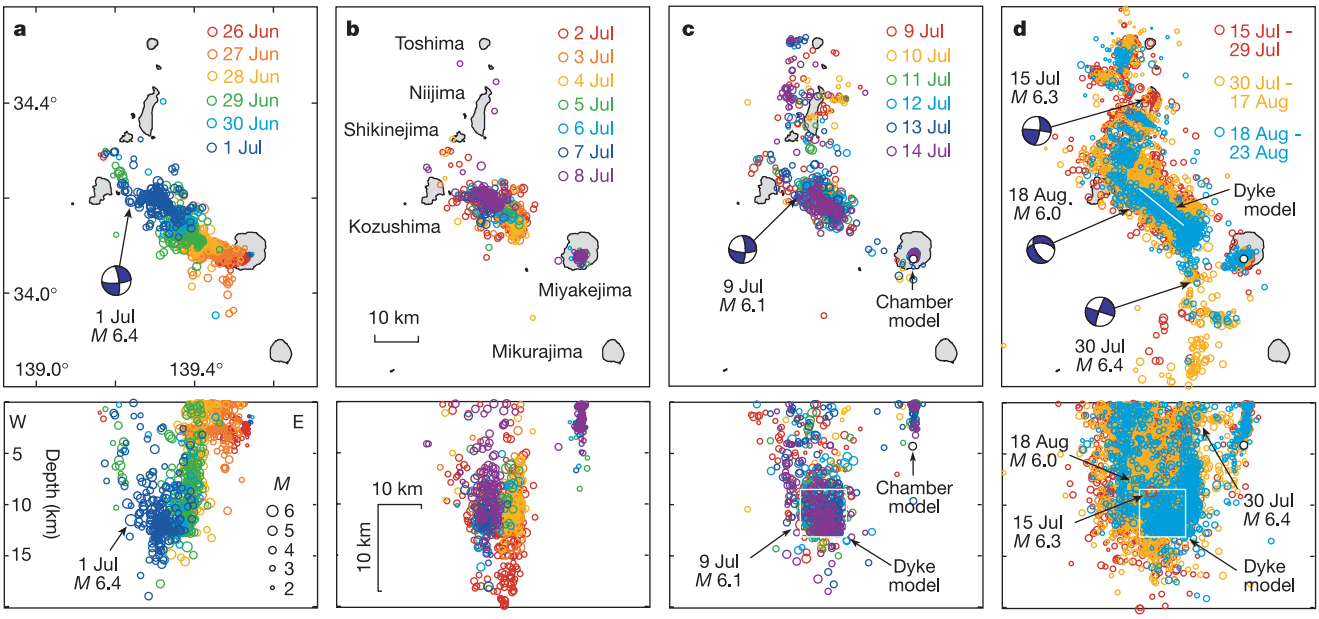

Figure 1 Swarm evolution in map view (top panels) and cross-section (bottom panels). Data from Earthquake Research Institute, University of Tokyo (ERI). Off-dyke seismicity appears within 3 d (**a**), and expands substantially after two weeks (**b**–**d**). Geometry of the inferred dyke and magma chamber is shown in **c**, **d**.